ORIGINAL ARTICLE

An integrated hybrid methodology for estimation of absorptivity and interface temperature in laser transmission welding

Dhruva Kumar Goyal[1] · **Ramsingh Yadav**[1] · **Ravi Kant**[1]

Abstract

This study reports a new hybrid integrated technique to predict the absorptivity of absorber and the interface temperature of the joint in laser transmission welding. The new approach is more robust as the numerical model is confirmed through experimental observations initially with weld width and further with surface temperature. Experiments are performed on polycarbonate sheets with electrolytic iron powder (EIP) as an absorber. The surface temperature and weld width are measured from the experiments. A transient 3-D finite element-based numerical model is developed for heat transfer analysis. The variation of heat flux with stand-off distance is also considered to enhance the accuracy of the computed results. The absorptivity is tuned in the numerical model by inverse analysis so that the numerical weld width is in close conjunction with the experimental weld width. After inverse estimation, the numerical model is validated with the experimental results of surface temperature using infrared thermography. The results indicate that the upper surface temperatures at the center in the numerical model are found to be in good agreement with experimental observations, and the average error is obtained to be less than 6%. Then, the interface temperatures are estimated after the validation of the numerical model.

Keywords Laser transmission welding (LTW) · Electrolytic iron powder (EIP) · Absorptivity · Finite element model · Interface temperature · Inverse estimation

1 Introduction

Laser transmission welding (LTW) is an innovative method to join polymers as it has several advantages over its contemporary joining methods [1, 2]. It is a fast, non-contact, non-contaminated joining process with high flexibility, automation, easy to control, consistent quality, and product stability [3]. In addition, this process can produce a high-quality joint with low thermal and mechanical stresses with a narrow seam geometry [4]. These qualities of LTW make it possible to broaden its applications in the field of automobile components, electronic and medical devices, and food-packaging industries [5].

A defocused laser beam passes through the upper substrate, which is transparent to the laser wavelength. When the laser beam reaches the interface, it is absorbed by the absorber and transformed into heat. Clamping pressure is critically required for the proper contact of surfaces as the heat at the interface can melt the polymers by thermal conduction. The combined effect of pressure and temperature results in the diffusion of polymeric chains, and joining of the polymer sheets occurs after solidification. Therefore, measuring the temperature at the interface is critical to verify the melt pool [6]. The temperature should be enough to ensure the joining of the substrates but not be too high, otherwise, degradation near the interface of the workpiece can occur [7].

In LTW, a lap joint configuration is widely used. However, temperature field investigation at the interface is difficult to monitor in lap joint configuration. Measuring interface temperature using thermocouples is also unsuitable because of the variation in thermal conductivity and absorptivity of thermocouple wires [8]. Pyrometer is an inexpensive, simple, and non-contact type method to measure the temperature at the interface, however, the heat emitted at

✉ Ravi Kant
 ravi.kant@iitrpr.ac.in; only4ravikant@gmail.com

 Dhruva Kumar Goyal
 2018MEZ0007@iitrpr.ac.in

 Ramsingh Yadav
 2018mez0006@iitrpr.ac.in

1 Department of Mechanical Engineering, Indian Institute of Technology Ropar, Rupnagar, Punjab 140001, India

the joining zone should be high enough, which must be susceptible to different wavelengths [9]. Infrared (IR) thermography is a real-time thermal monitoring method used in laser transmission welding. IR thermography measures the temperature field distribution at the surface of the object by emitting the radiation at the time of welding [10]. Due to the optical envelop at the interface, it cannot provide thermal information of the joining zone. Therefore, the researchers have developed numerical models to investigate the interface temperature in the LTW process [11].

Becker and Potente [8] established a model to analyze the melt profile in the heating phase of LTW in the contour welding of polypropylene. Van De Ven and Erdman [12] developed a 2-D heat transfer model for thermal analysis in LTW of PVC. Mahmood et al. [13] developed an FEA-based analysis to get the temperature distribution at different process parameters by comparing it with weld width obtained experimentally. Mayboudi et al. [14] developed a 3-D FE-based thermal model to investigate the heating and cooling stages in LTW by a moving laser beam source and overcome some assumptions made in previous models. Acherjee et al. [15] developed a 3-D FEM model to investigate the effect of carbon black content in weld profile with temperature-dependent thermal properties. Sooriyapiragasam and Hopmann [16] developed a thermo-mechanical simulation model for spatial temperature and stress distribution in weld seam. Liu et al. [1, 2] created a finite element model to analyze the role of thermal conductivity of metal absorber in the weld seam and temperature distribution. Wang et al. [17] developed a finite element-based model to investigate the effect of thermal contact conductance. The temperature distribution and the weld width were found in excellent agreement with experimental results. Acherjee [18] developed a 3-D FE-based model for LTW of dissimilar plastics. The dilution effect at the weld pool was considered in simulation and found that it affected the maximum temperature zone.

Literature reports a number of numerical models which consider the tuned absorptivity. Most of these models are not validated with the experimental temperature field. These models may not be able to predict the process outcomes accurately for a wide range of parameters. Incorporation of effective absorptivity and validation of the model with actual temperature field can make the model reliable and accurate for a wide range of process conditions. In this paper, a hybrid integrated approach which is based on experiments, numerical analysis, and inverse estimation approach has been developed to estimate the absorptivity and interface temperature for lap joint configuration in LTW. For this purpose, experiments are carried out at different process parameters, i.e., laser power and scanning speed. In experiments, the temperature has been measured by the infrared camera and weld width by tool maker microscope. A 3-D

finite element model is developed to validate the results and estimate the temperature at the interface.

2 Materials and methods

2.1 Methodology

The experiments of LTW are conducted to join PC workpiece with electrolytic iron powder (EIP) at different process parameters. The flow chart of the procedure to find the interface temperature is shown in Fig. 1. In-process thermal field distribution over the top surface of PC is measured through infrared (IR) thermography. Weld width of the workpiece joint is measured by a tool maker microscope. A three-dimensional finite element model is developed for transient thermal analysis. Weld width in the numerical model is compared with the experimental weld width. Numerical weld width is a function of temperature-dependent thermal properties of PC, applied boundary conditions, and absorption of the irradiated laser beam at the interface. The numerical model consists of temperature-dependent material properties, and boundary conditions are applied as per the real-time condition of the workpiece. The only parameter which is unknown and can affect the weld width significantly is the absorptivity. The bisection method is used for tuning the absorptivity in the numerical simulations. The absorptivity is considered when the difference between experimental and numerical values of weld width approaches less than 0.1 mm. After this, validation of the numerical model is done by comparing the top surface temperature obtained from the numerical model with the experimental temperature by IR camera. The validated model is then used to estimate maximum temperatures at the workpiece interface.

2.2 Experiments

The experiments are performed on a polycarbonate sheet (70 mm × 30 mm × 2 mm). CO_2 laser cutting machine (ELITA 480, MEHTA CAD-CAM, INDIA) was used for sample cutting. Polycarbonate specimens are cleaned by using ethyl alcohol of purity 90% to remove dust, foreign particles, and decoloration effect during the cutting of specimen by CO_2 laser. The transmittance and absorbance of the polycarbonate with respect to air are measured using ultraviolet visible near-infrared spectroscopy (UV–VIS-NIR, UV-2700 SHIMADZU, JAPAN), in the range of 800–1400 nm. These are required for numerical simulations to determine the temperature in the joining zone. The results of transmittance (τ) and absorbance (α) of polycarbonate are shown in Fig. 2. The reflectance (Φ) of the polycarbonate substrate can be calculated from Eq. (1).

Fig. 1 Flow chart represents the development and calibration of interface temperature in laser transmission welding
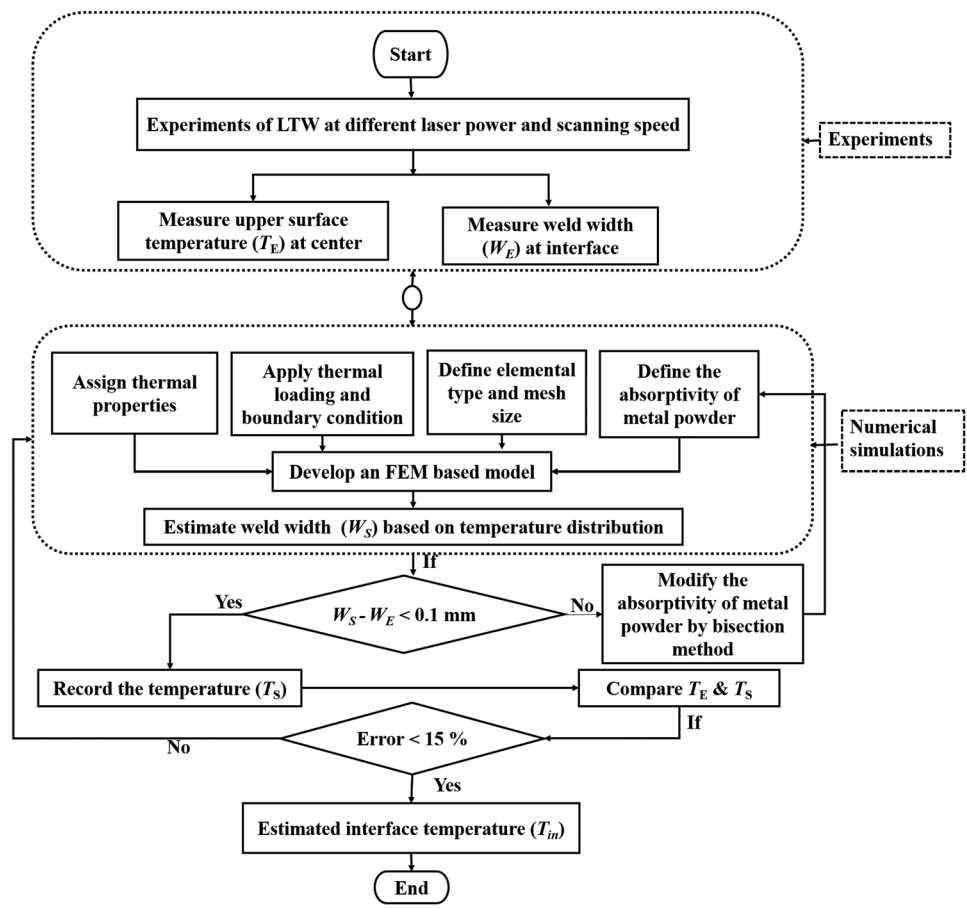
$$\phi = 1 - \tau - \alpha \qquad (1)$$

EIP particles of 500 mesh size are used as an absorber which is applied along the travel length of the laser beam. The SEM image of EIP particles is shown in Fig. 3. In the overlap region of the lower PC sheet, ethanol is applied,

and iron powder particles are spread over this region. The gravitational effect removes the excess powder particles by placing the PC sheet vertically. A layer of powder particles is developed over this surface. Furthermore, the spatula is used for leveling the powder layer, and uniformity is ensured by visual inspection. After that, the PC sheet is air-dried for 2 h

Fig. 2 Transmittance and absorbance of polycarbonate at 800- to 1400-nm wavelengths measured by UV–VIS-NIR
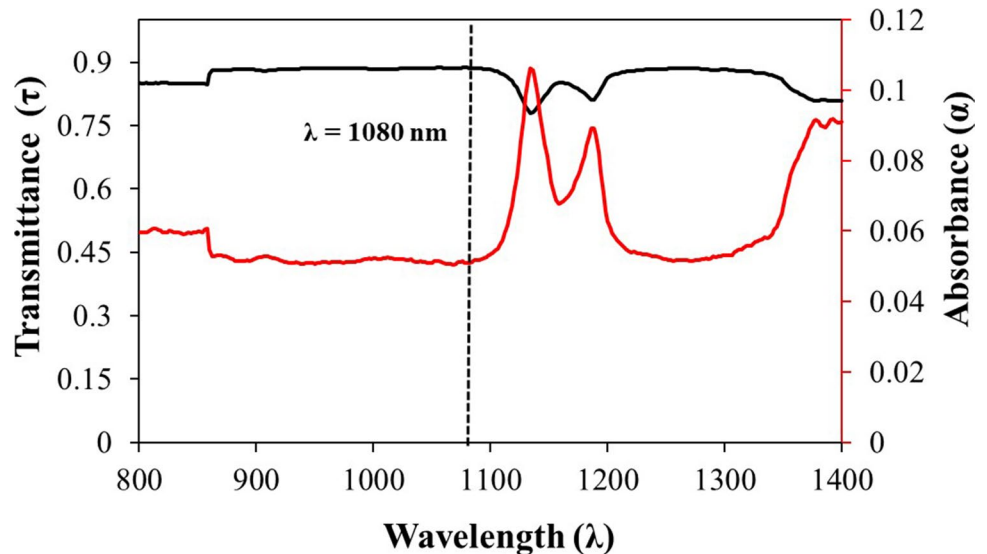
Fig. 3 SEM image of EIP particles

to evaporate the ethanol from the surface. The EIP particles are applied at the overlap region within the range of 0.3- to 0.4-g weight. For this purpose, the weight of the sample is measured after disposing the EIP layer and subtracted from the initial sample weight. The weight of the sample is measured by the weighing scale (SES 300, SAFFRON, INDIA).

The experiments on transmission welding are performed using a 1000 W fiber laser source (MAX-MFSC-1000 W, CW) system with a wavelength of 1080 nm. The laser head is mounted on a computer-controlled 3-axis CNC system for the precise speed and position of the laser beam. At 1080-nm wavelength, the PC sheet is found to transmit 90% and reflect 5% of the total incident laser beam energy, as shown

in Fig. 2. The stand-off distance (63 mm) is determined precisely by the CNC control system after altering the distance from the PC upper surface to the nozzle tip in the laser head. A beam diameter of 6 mm is considered for more uniform power distribution, according to the published literature [19]. The PC workpieces are placed in a lap joint configuration between four plates of mild steel of 60 mm × 15 mm × 5 mm, as shown in Fig. 4. The experimental setup and position of the camera is shown in Fig. 5a. Clamping pressure of 3 MPa is applied for proper contact between PC substrate and iron powder so that heat can transfer through conduction. A hydraulic system applies the pressure, and uniform pressure is ensured by reading on the pressure gauge. The clamping arrangement with hydraulic jack, the position of PC sheets after clamping, and a pressure gauge are shown in Fig. 5b, c, and d. The laser beam irradiation is started and stopped at 10 mm away from the sheet so that the effect of acceleration and deacceleration of the moving parts can be avoided.

The surface temperature is measured by IR camera (A315, FLIR, SWEDEN) at the time of experiments. This IR camera is equipped with a lens of 18-mm focal length and characterized for the spectral range 7.5–13 μm. The IR camera is placed at 0.5-m distance from the sheets at an angle of approximately 45°. The frame rate to capture the temperature of the upper surface of polycarbonate is taken as 60 Hz. The temperature range is set at 0–500 °C because PC starts to degrade above this temperature.

A tool maker microscope (RTM-900, RADICAL, INDIA) with a magnification of 15 × is used to investigate the weld width and internal morphology of the joint at different process parameters. Weld width is measured at the three

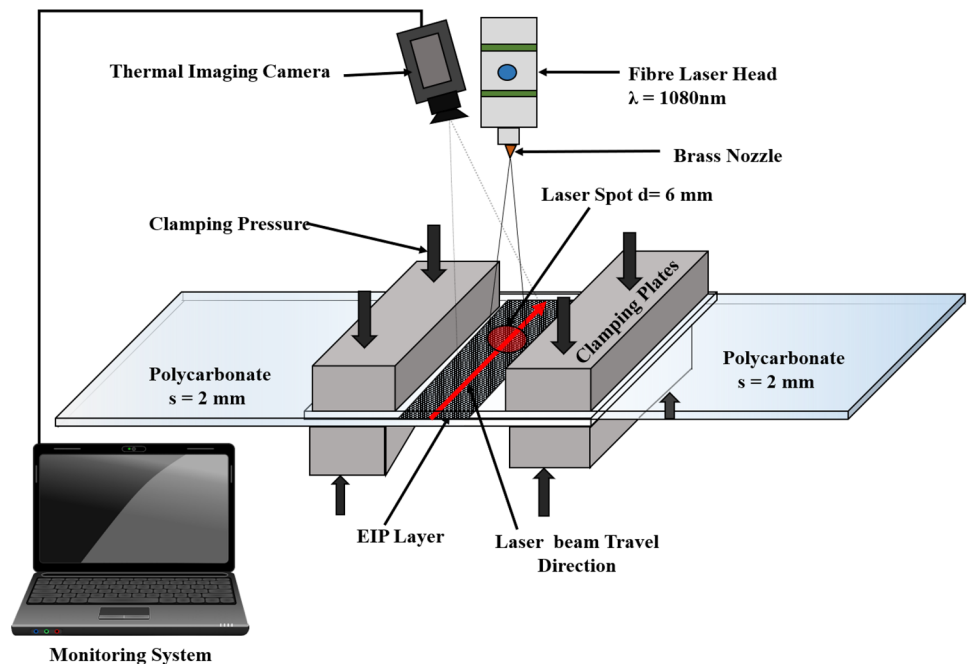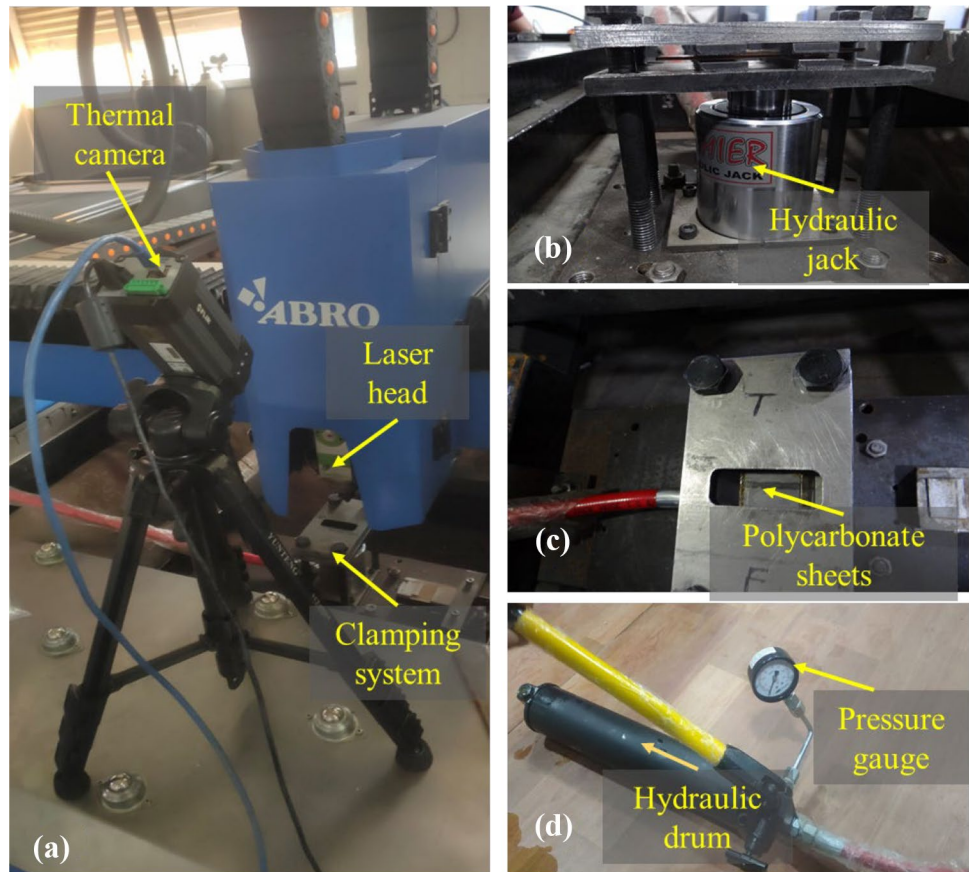**Fig. 4** Schematic diagram of experimental setup for LTW of polycarbonate sheet

Fig. 5 **a** Experimental setup and position of IR camera, **b** clamping arrangement with hydraulic jack, **c** PC sheet position, **d** pressure gauge

different points along the weld length, and an average of these weld widths has been taken. The experiment plan at different levels of laser power and scanning speed is listed in Table 1. Two replications have been performed for each combination of laser power and scanning speed.

2.3 Numerical modeling of LTW

Thermal analysis of laser transmission welding of polycarbonate is carried out by finite element analysis using ABAQUS software. The geometry and dimensions of substrates are shown in Fig. 6. The temperature-dependent thermal properties are shown in Table 2. Due to symmetry in geometry and material properties, half of the model is considered for the current analysis to reduce the simulation time. The interaction time of the laser beam at the interface is very less, and heating in a narrow region also favors the

Table 1 Experimental plan: process parameters and their levels

| Parameters	Level 1	Level 2	Level 3	Level 4
Laser power (W)	80	100	120	150
Scanning speed (mm/min)	200	400	600	-

above consideration. The following assumptions are considered in the development of the FEM model:

1. Material is considered to be homogeneous and isotropic.
2. The laser beam is assumed circular and follows the Gaussian distribution of intensity.
3. There is perfect contact between the substrates.
4. Iron powder is considered a flat layer at the upper surface of the nether PC only to absorb the laser energy.
5. The thermal conduction between iron particles is neglected due to lack in a continuous distribution of iron powder. The effective thermal conductivity of iron powder decreases as the distance between iron particles increases because it enhances the thermal contact resistance.
6. The thermal conduction between iron particles and PC walls occurs at the interface. The thermal conductivity of iron powder particles is much larger than PC and the contact area is also less than the actual interface area. Therefore, the contact thermal conductance is assumed very high at the interface [20].
7. Heat capacity of iron particles is also neglected in the simulation because small mass of EIP particles is applied at the interface.

Fig. 6 Schematic view of dimensions, boundary conditions, and beam direction used in lap joint
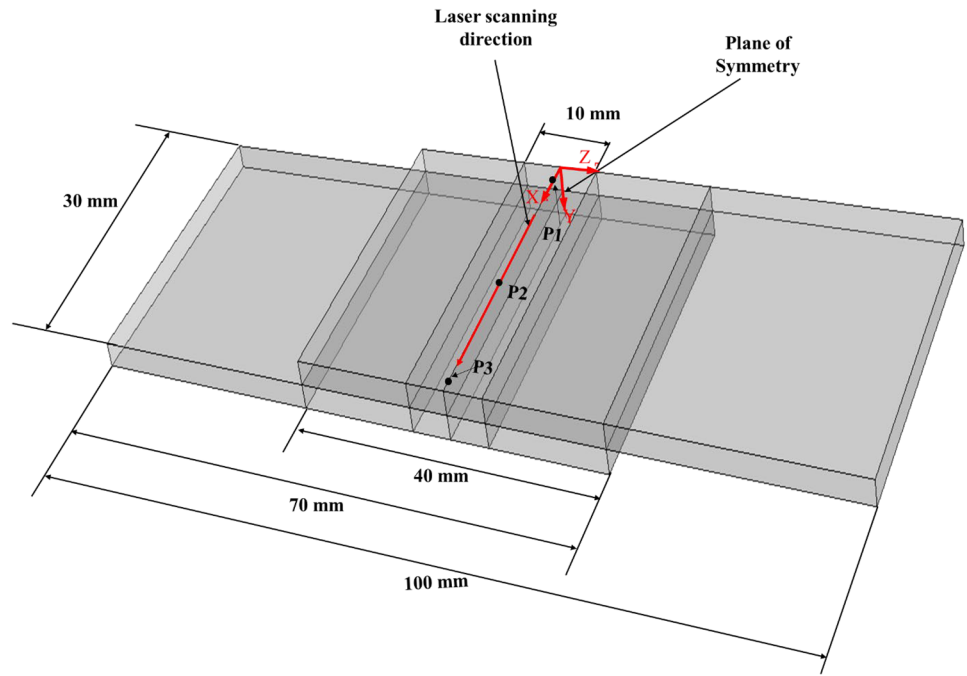
2.3.1 Laser beam model

A continuous wave laser heat source is moving with uniform velocity (V) along the weld line. The laser beam has a Gaussian heat flux distribution inside the beam diameter. The PC sheet transmitted 90% and absorbed 5% of the total radiation, and the rest is reflected. The PC sheet absorbs the radiation along with the thickness(s); therefore, volumetric heat flux is applied in the model for laser beam interaction with PC along the weld line [24]. The volumetric heat flux (Q_v) is described by Eq. (2) as:

$$Q_v = \frac{(1 - \phi)\alpha_v 2P}{\pi R^2 s} \exp\left(-\frac{2\left((x - V * t)^2 + z^2\right)}{R^2}\right), \quad (2)$$

where P is the average laser power, x and z are the coordinates of the laser beam along the weld length and width respectively, Φ is the reflectivity, and t is the time. The volumetric absorptivity coefficient, α_v, is taken as 0.05 and R is beam spot radius.

The laser beam is transmitted through the PC sheet and irradiates iron particles. The heat flux is absorbed by these particles, termed as surface heat flux (Q_s), represented by Eq. (3) as:

$$Q_s = \frac{\alpha_s \tau 2P}{\pi R^2} \exp\left(-\frac{2\left((x - V * t)^2 + z^2\right)}{R^2}\right), \quad (3)$$

where α_s is the effective absorptivity of iron powder, and τ is the transmissivity of upper PC sheet which is taken as 0.9, obtained from the results of Fig. 2. It is because 90% of the laser beam energy is available to absorb at the interface. Laser beam spot can be controlled by adjusting the distance from the focal point (set at the nozzle tip) to the workpiece surface. The spot radius of the laser beam at the

Table 2 Temperature-dependent thermal properties of polycarbonate used in numerical modeling [17]

Properties	Value	Condition
Density (ρ) (kg/m³)	$\rho = -0.319\,T + 120$	$27 \leqslant T \leqslant 145\,°C$
	$-0.685\,T + 1253$	$T > 145\,°C$
Thermal conductivity (k) (W/m–K)	$k = (2.493E - 4)\,T + 0.186$	$27 \leqslant T \leqslant 145\,°C$
	$-(5.536E - 5)\,T + 0.23$	$T > 145\,°C$
Specific heat capacity (c) (J/kg-K)	$c = 3.42\,T + 1120.67$	$27 \leqslant T \leqslant 140\,°C$
	$27.385\,T - 2236.38$	$140 \leqslant T \leqslant 147\,°C$
	$1.771\,T + 1537.41$	$T > 147\,°C$
Glass transition temperature (T_g) (°C)	145–150 °C	
Flow temperature (T_f) (°C)	230–240 °C	
Decomposition temperature, (T_d) (°C)	550 °C	

Fig. 7 Meshed part used in numerical simulation
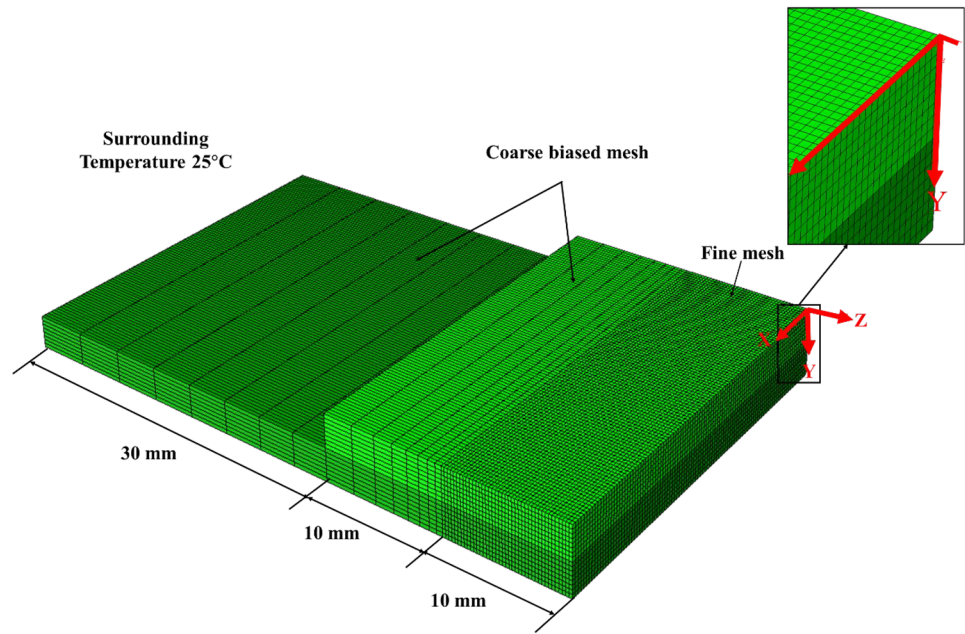
stand-off distance H from the focal point can be described by the mathematical model [21] as shown below:

$$R = w_o \sqrt{1 + \left(\frac{M^2 \lambda (H + y)}{\pi w_o^2} \right)} \quad (4)$$

where $w_o = 10 \mu m$ is the beam waist radius at the focal point, λ is the wavelength of the laser beam, and y is the depth of the workpiece. M^2 is the beam quality factor. For a perfect Gaussian beam, the value of the beam quality factor is taken 1. But, in this analysis, beam quality factor is calculated analytically by Eq. (5) as shown below:

$$M^2 = \frac{\pi w_o \theta_d}{\lambda}, \quad (5)$$

where θ_d is the half divergence angle which can be calculated by:

$$\theta_d = \frac{R_0}{f}, \quad (6)$$

where f is the focal length of the lens used to focusing the laser beam, equal to 125 mm, and R_0 is the radius of the laser beam before the lens. By putting Eq. (6) in Eq. (5), we can get the value of $M^2 = 1.39$.

2.3.2 Heat flow model

The laser energy is absorbed and generates heat at the interface. The heat is transferred between the substrates mainly through thermal conduction. The spatial and temporal temperature field is determined by a 3-D heat conduction equation. It is based on the energy conservation law, which balances the rate of heat generated internally in the body, the

Fig. 8 Calibration of emissivity of polycarbonate surface: **a** infrared measurement, **b** comparison of thermocouple and infrared temperature at different emissivities
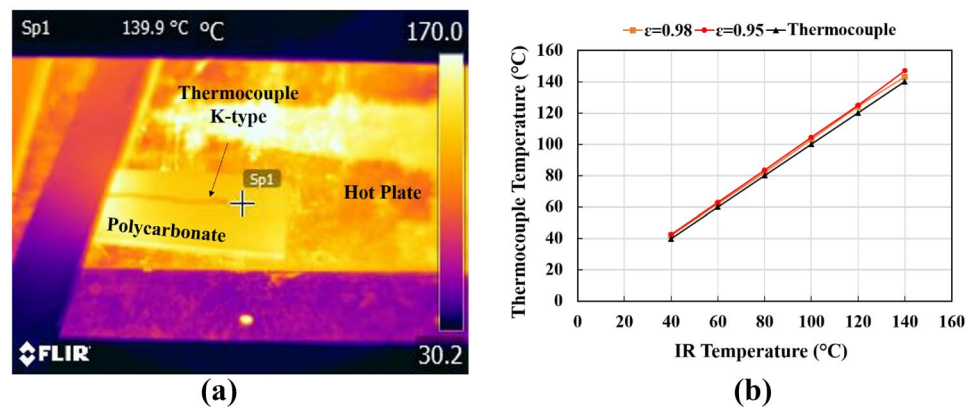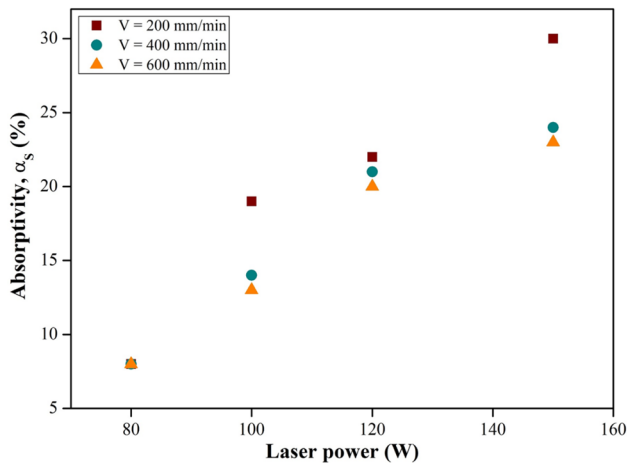
Fig. 9 Variation of absorptivity with laser power at different scanning speeds

capacity of the body to store the heat, and the rate of heat conduction to the boundaries.

$$\frac{\partial}{\partial x}\left(k\frac{\partial T}{\partial x}\right) + \frac{\partial}{\partial y}\left(k\frac{\partial T}{\partial y}\right) + \frac{\partial}{\partial z}\left(k\frac{\partial T}{\partial z}\right) + Q(x,y,z,t) = \rho c_p \frac{\partial T(x,y,z,t)}{\partial t}, \tag{7}$$

where k is the thermal conductivity; c_p is the specific heat; T is the temperature; Q is the heat generated per unit volume; x, y, and z are the Cartesian coordinates; and ρ is the density.

Heat loss from the surface exposed to the surroundings is primly due to natural convection. The boundary condition for heat transfer by convection is defined by equation

$$q_{conv} = h(T_n - T_o), \tag{8}$$

where h is the heat transfer coefficient. T_n is the node temperature and T_o is the surrounding temperature taken as 25 °C. The radiation heat loss is neglected concerning conduction and convection.

2.3.3 Model description

A 3-D FEM-based heat transfer model is developed for the analysis of temperature in the weld zone by using an ABAQUS/standard solver. An 8-node linear heat transfer brick element DC3D8 is used for the analysis. The region prone to a significant portion of laser power is discretized into a finer mesh region of element size $0.25 \times 0.25 \times 0.25$ mm. The region away from the heated region is discretized in biased coarser mesh to reduce the computational time, as shown in Fig. 7.

The moving body heat flux at the upper PC and surface heat flux at the nether PC is applied through a user-defined DFLUX subroutine. A single, self-adaptive time step is used to perform the thermal analysis. In this step, initial time is given for the heating phase and later for

Fig. 10 Optical images at the center of the lower PC sheet: **a** P = 80 W and V = 600 mm/min, **b** P = 100 W and V = 400 mm/min, **c** P = 120 W and V = 400 mm/min, **d** P = 150 W and V = 200 mm/min
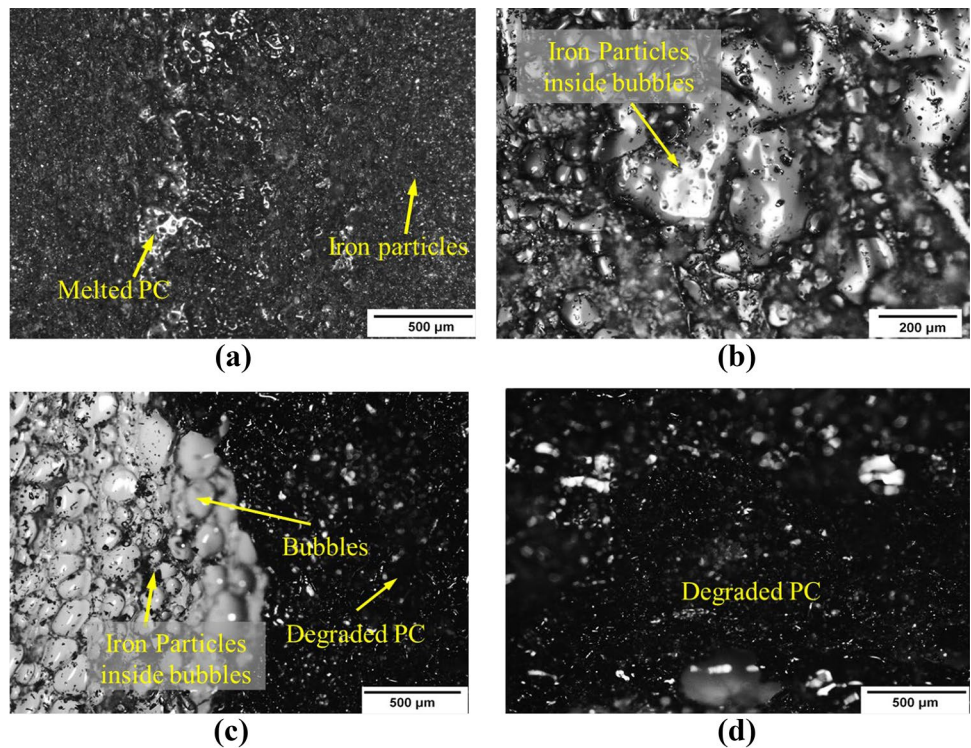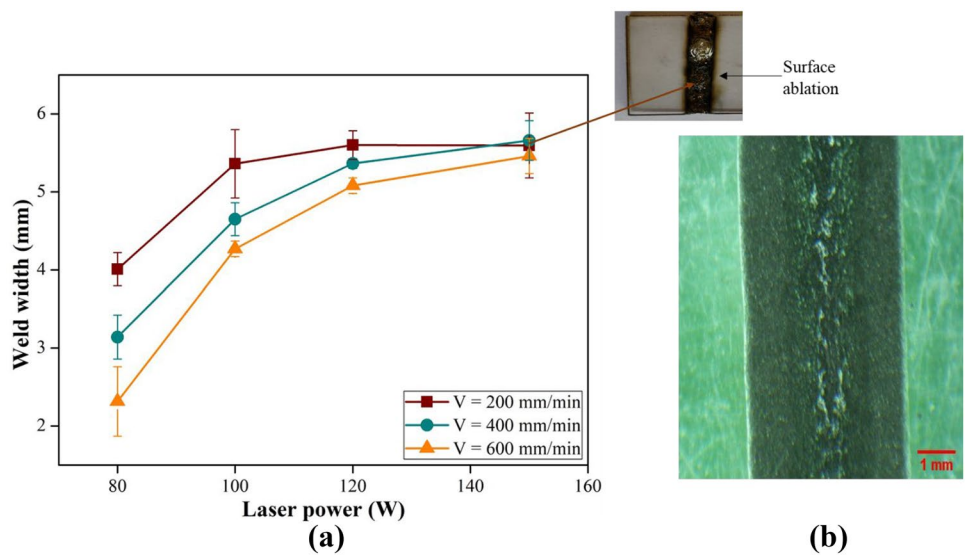
Fig. 11 Variation of weld width with **a** laser power at different scanning speeds and **b** weld width measured in the tool maker microscope for P = 80 W and V = 200 mm/min

(a)

(b)

cooling of the substrate. The maximum and minimum time steps were taken as 2 s and 5×10^{-5} s, respectively. Maximum allowable temperature change per increment is taken as 30 °C by sensitivity analysis for optimal step time increment.
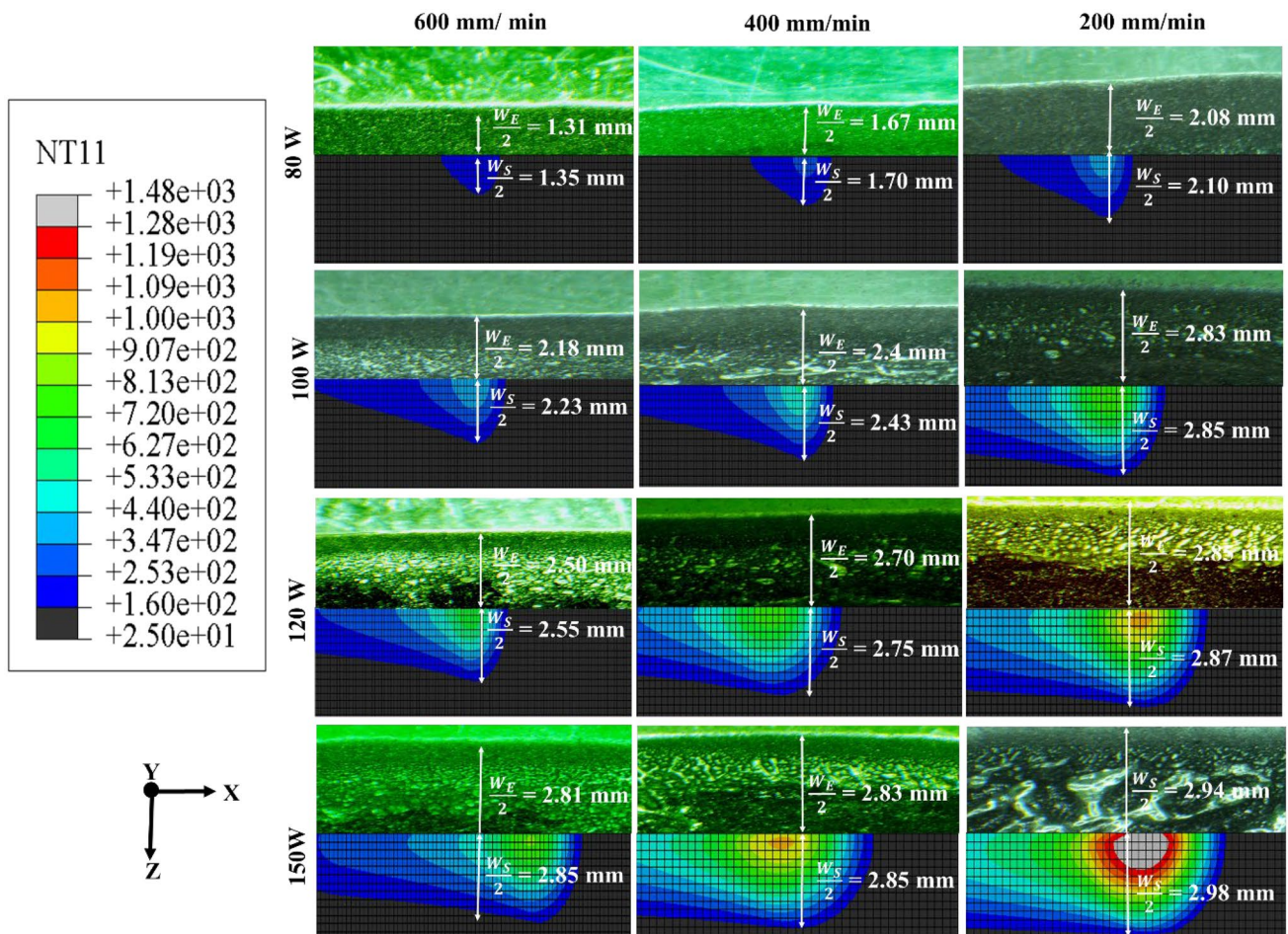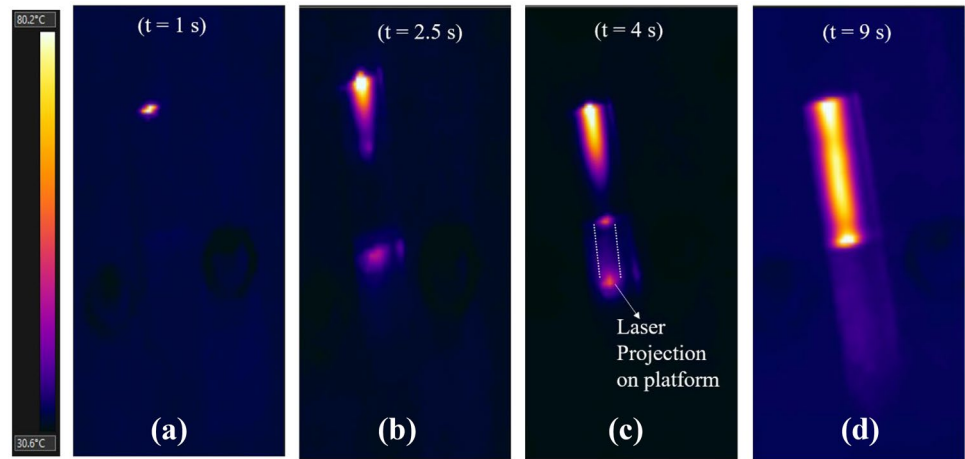

Fig. 12 Comparison of experimental weld width measured with a tool maker microscope and simulated weld width measured with temperature profile

Fig. 13 IR measurement of top surface temperature of PC at different time intervals for $P = 100$ W and $V = 600$ mm/min

3 Results and discussions

3.1 Calibration of emissivity

A fine emissivity of polycarbonate surface is essential for the quantitative measurement of temperature by infrared thermography. For this purpose, the polycarbonate sheet is heated by placing it on a hot plate. In addition, a K-type thermocouple is attached to the top surface of the PC sheet, connected with a data acquisition (DAQ) system to get a real-time temperature. The infrared camera is focused at a point (Sp1) on the surface of the polycarbonate by choosing the arbitrary emissivity to show the room temperature, as shown in Fig. 8a. The plate is heated in a step of 20 °C from room temperature to 150 °C.

The temperature is recorded in the DAQ system when it reaches at a steady-state condition. Thermocouple temperature is compared with the infrared measured value at different emissivities to get a close temperature value as measured by a thermocouple. It is observed that surface temperature

is in good agreement with an average error < 2% for the infrared emissivity at 0.98, up to 140 °C as shown in Fig. 8b. The hot plate is not heated above 150 °C as above this temperature workpiece started to lose its shape.

3.2 Calibration of absorptivity of iron powder

It is important to provide a calibrated property to a finite element-based model to predict the temperature of the interface at the joining zone. The absorptivity is such an important parameter that directly affects the heat generated by the absorber. The absorptivity of a substance depends on the laser wavelength, process conditions, concentration, temperature, shape, and size of the absorber. Laser beam falls on the iron particles, a part of the laser beam is absorbed by the iron powder particles and transmitted through the micropores remaining after the coating, and the rest is reflected. Therefore, an inverse analysis has been done for measuring the effective absorptivity at different process conditions. For each process condition, the experimental weld width (W_E) is

Fig. 14 Variation of the upper surface temperature of PC with time at three different laser beam positions at the P1, P2, and P3 for $P = 100$ W and $V = 600$ mm/min
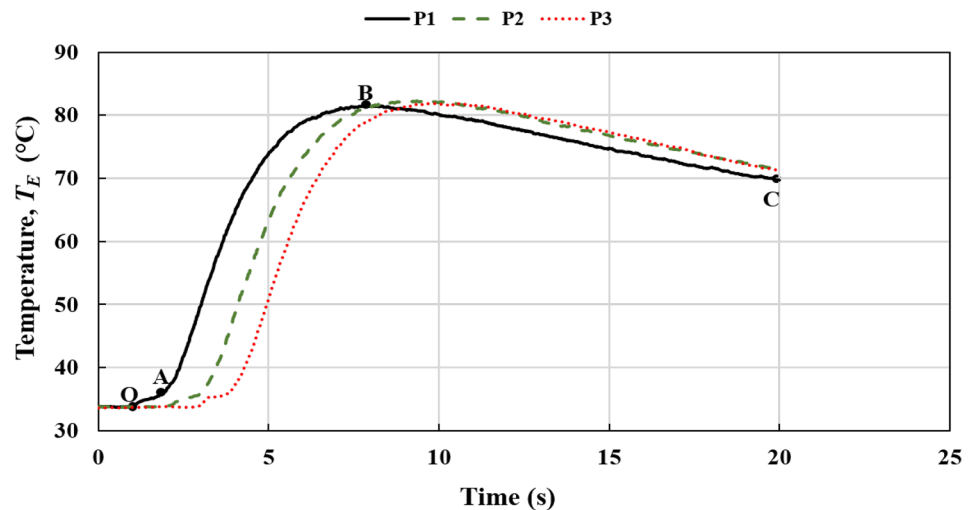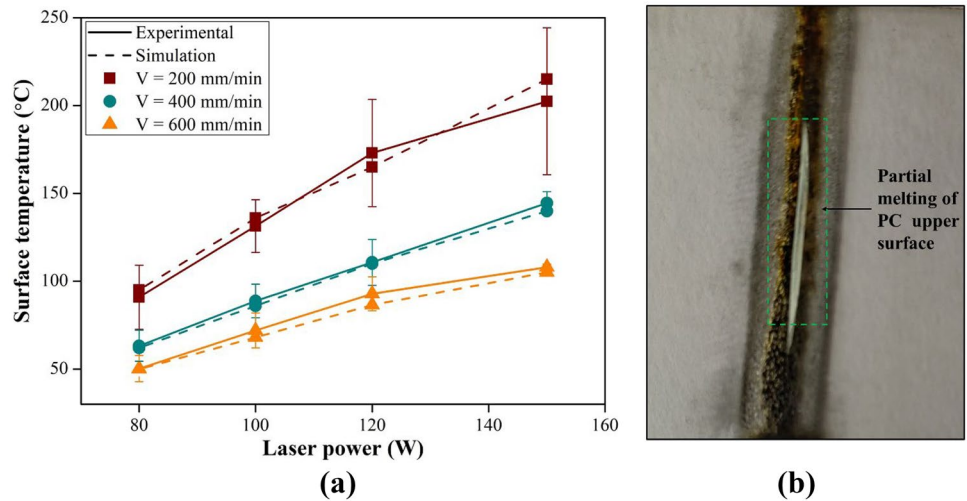
Fig. 15 **a** Variation of top surface temperature at the center of PC with power at different cutting speeds in experiment and simulation, **b** upper PC surface at $P = 120$ W and $V = 200$ mm/min

(a)　　　　　　　　　　　(b)

measured and compared with simulation weld width (W_S) by adjusting absorptivity so that the difference in their values lies less than 0.1 mm. The results of absorptivity at different process conditions are shown in Fig. 9.

The absorptivity increases with increasing the laser power and decreasing the scanning speed. It may happen because as the laser beam irradiates, the temperature at the interface increases, which melts the PC at the interface. The absorptivity is almost constant with scanning speed at low laser power (80 W), as the generated temperature is less than the melting temperature of PC. Furthermore, at high scanning speed, the laser beam is irradiated for a shorter time, which reduces the diffusion of laser beam energy into the iron particles and decreases the absorptivity. The optical micrographs at the lower PC interface are shown in Fig. 10. At low laser power ($P = 80$ W) and high scanning speed ($V = 600$ mm/min), a small melt pool of PC is developed, as shown in Fig. 10a. However, increasing the laser power ($P = 100$ W) and decreasing scan speed ($V = 400$ mm/min) encourages the formation of bubbles in the melt pool due to the increase in the available energy for absorption. Some iron particles are also present inside the bubbles, as shown in Fig. 10b. The reflected laser beam from iron particles may interact and reflect from the inner surface of bubbles in PC. Then, it may be further absorbed by the iron particles which results in increment of the absorptivity. Wahba et al. [22] also observed a similar phenomenon during laser-assisted joining of amorphous polyethylene terephthalate with AZ91D thixomolded Mg alloy. With further increase in power ($P = 120$ W) at similar scanning speed ($V = 400$ mm/min), the partial degradation of PC occurred and large bubbles are generated in the heat-affected zone. Large bubbles may have more iron particles which absorb the reflected laser energy as shown in Fig. 10c. The thermal degradation of PC also improves absorptivity of iron powder [23]. Severe thermal degradation occurred at high

laser power ($P = 150$ W) and low scanning speed ($V = 200$ mm/min) as shown in Fig. 10d. The higher absorptivity may be due to the severe thermal degradation and softening of the iron particles.

3.3 Weld width

The effect of laser power on weld width at different scanning speeds is shown in Fig. 11a. At all scanning speeds, the weld width increases with laser power due to more heat absorption at the interface. The weld width, measured by tool maker microscope at $P = 80$ W and $V = 200$ mm/min, is shown in Fig. 11b. One exception case of decreasing weld width is found at a low scanning speed of 200 mm/s and high power of 150 W. At these parameters, the laser beam is absorbed by the upper surface of the PC and started the degradation or burning of the workpiece. The average weld width is decreased with increasing the scanning speed. This
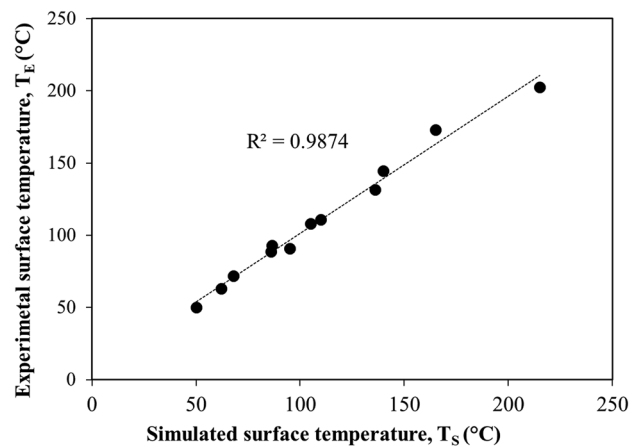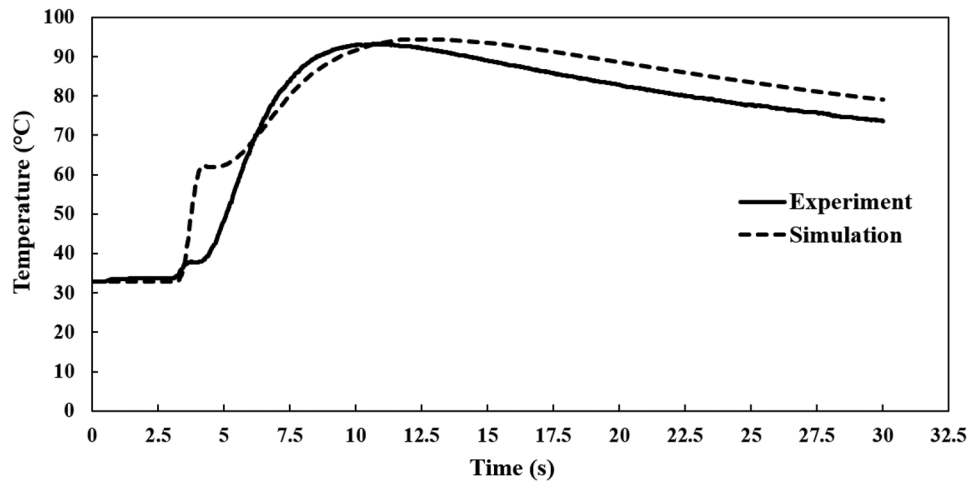

Fig. 16 Comparison of experimental and FE-based model predicted temperature of PC surface

Fig. 17 Comparison of experimental and simulated top surface temperature at the center with time at $P = 100$ W and $V = 400$ mm/min

is due to the fact that by increasing the scanning speed, the time of laser beam interaction with the EIP is decreased, which reduces the amount of heat generated at the interface. The difference in weld width is more at different scanning speeds at low power compared to high laser power. This is due to the fact that at low laser power, more non-uniform welding is obtained along the scan line.

At the time of measurement of weld width, it is assumed that the joining process started when the temperature at interface reached 160 °C, above the glass transition temperature of PC ($T_g = 150$ °C). The weld width measured experimentally and by numerical simulation is compared as shown in Fig. 12. As the minimum width of the element is 0.25 mm and the maximum error is restricted below 0.1 mm, an image processing software has been used to achieve high accuracy. This is seen that the maximum weld width, W_E, is lower than the beam diameter ($d = 6$ mm) of the laser beam.

3.4 Temperature analysis

Since PC is opaque in the IR range, therefore, it provides the temperature reading of the upper surface of PC. The temperature distribution along the weld length at different time intervals for $P = 100$ W and $V = 600$ mm/min is shown in Fig. 13. The laser beam interacts with the PC sheet at the start, middle, and end point of the scanning length at t=1, 2.5, and 4 s respectively (Fig. 13a-c). The maximum temperature at the surface of the PC sheet is reached after 5 s of passing the laser beam, i.e., at t=9 s (Fig. 13d). The measured values of temperature with time at different positions are represented in Fig. 14. It is observed that the high temperature at the top surface of PC is reached after some time of laser irradiation. It is due to the fact that the laser is absorbed at the joining interface for a very short time on the iron powder and the PC has very less thermal conductivity. For better understanding, this temperature distribution can be divided into three regions. In the first irradiated region, O-A, a very small initial

temperature rise occurs and is maintained constant till the time of interaction. Thereafter, it comes into the conduction zone, A-B, where the temperature increases continuously to a maximum and then decreases in the cooling phase in B-C.

3.5 Validation of numerical model and prediction of interface temperature

The temperature of the top surface of PC is measured by IR technique and compared it with the simulation temperature to verify the numerical model. The variation of the top surface temperature of polycarbonate at the center with power and scanning speeds and the comparison between numerical and experimental results are shown in Fig. 15. The data measured by simulation is nearly close to the experiment and fits very well with R^2 (98.74%) value approximate unity as shown in Fig. 16. The surface temperature increases marginally during the laser beam passing over a point on scan length and it further increases due to thermal conduction.
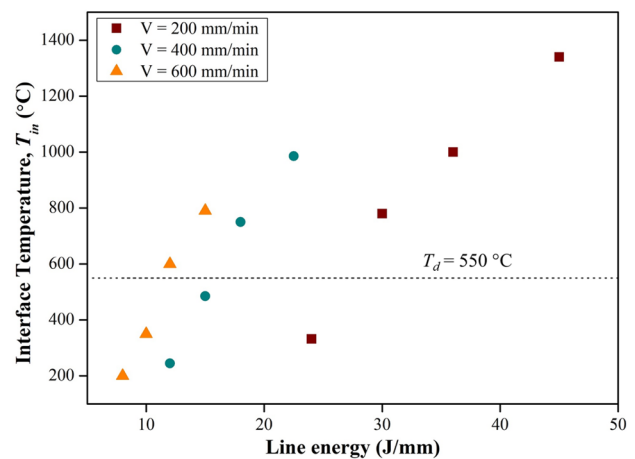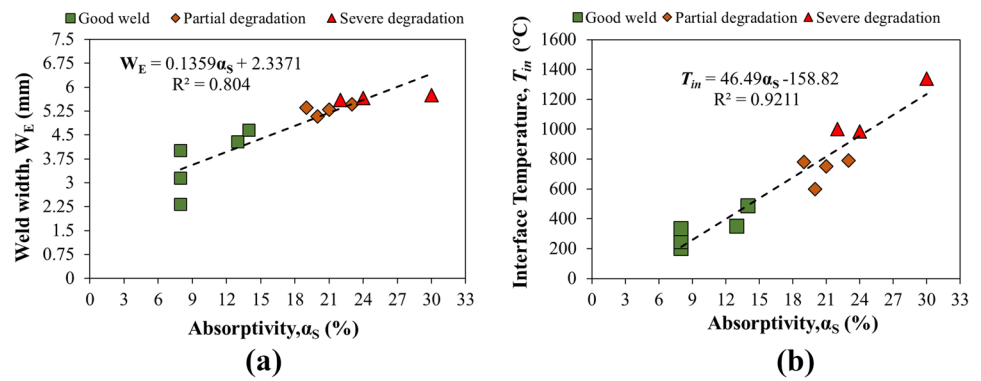

Fig. 18 Variation of interface temperature with line energy

Fig. 19 Influence of absorptivity on **a** weld width and **b** interface temperature for different qualities of joint

(a)

(b)

This is also observed in the simulation at $P = 100$ W and $V = 400$ mm/min, as shown in Fig. 17. In the numerical simulations, the temperature rise in the irradiation time zone (OA) is higher than in experiments, but it has obtained the peak temperature in nearly the same time.

The numerical model predicts the upper surface temperature at the center with a fine accuracy with an average error of less than 6%. An increase in error is observed (10–14%) in predicting the temperature when the surface temperature is reached above the glass transition temperature (150 °C) of PC. There may be several reasons for the error in estimating upper surface temperature, such as the assumptions that follow in the development of the FE model. Furthermore, the effect of temperature-dependent emissivity in IR is not considered; melt flow and its properties such as solidus and liquidus temperature are not considered in the numerical model. Partial melting of top PC surface at power, $P = 120$ W, and scanning speed, $V = 200$ mm/min, and temperature in simulation is near to flow temperature of PC which also confirms the validation of the numerical model.

After validation of the numerical model, the temperature at the interface is predicted by the numerical model with line energy as shown in Fig. 18. Line energy is the ratio of power to the scanning speed. At low line energy, the temperature at the interface is above the glass transition but lower than the flow temperature of polycarbonate. As the line energy increases from 8 to 15 J/mm, it reaches near the degradation temperature of PC.

It is observed that with an increase in line energy above 15 J/mm by increasing the laser power at constant scanning speed; the interface temperature is increased above the degradation temperature of polycarbonate. The degradation of the PC specimen at the center of the joint can be confirmed from Figs. 12 and 15b. The degradation temperature of a thermoplastic is dependent on the heating rate [19]. The combination of high laser power and low scanning speed generates enormous energy per unit length at the interface. A high temperature is maintained in the joining interface for a long time over a large area, as shown in Fig. 12, which leads to the degradation of polymers.

3.6 Effect of absorptivity on weld width and interface temperature

The weld width is increased with increasing the absorptivity of the EIP, as shown in Fig. 19a. It is because an increase in the absorptivity leads to an increase in the heat generation, which increases the interface temperature shown in Fig. 19b. The weld joint is discretized as good weld, partial degradation, and severe degradation based on the visual appearance of the weld seam. Good welds are observed for absorptivity between 8 and 15%, and weld width is reached up to 4.65 mm. It is because the interface temperature remains below the degradation temperature of PC. With further increase in the absorptivity, the interface temperature is increased above the degradation temperature of PC and leads to poor quality

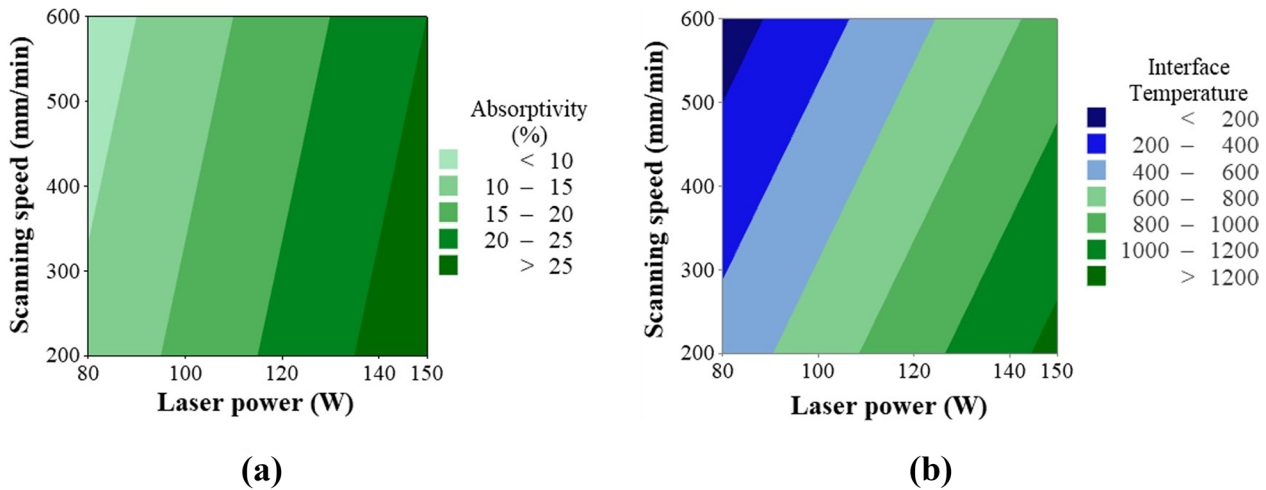**Fig. 20** Normal probability plot of the residuals for **a** absorptivity and **b** interface temperature

(a)

(b)
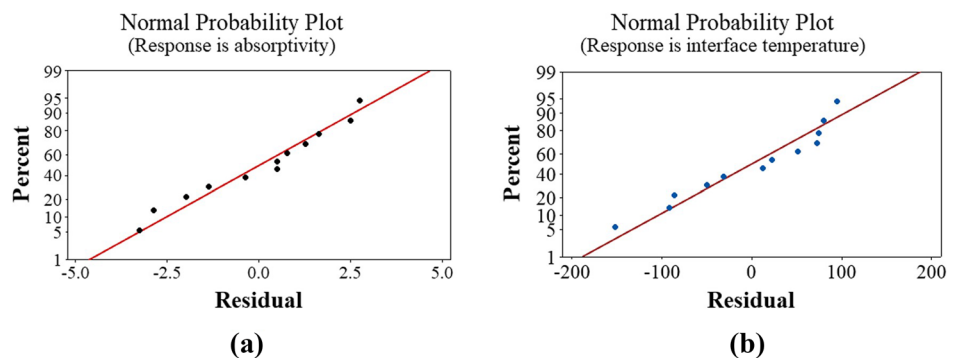
Fig. 21 Contour plots of laser power verses scanning speed for **a** absorptivity and **b** interface temperature

joint. The maximum weld width is obtained at 30% absorptivity because rapid increase in the interface temperature occurred, resulting into severe degradation at the interface.

4 Regression model

In the present study, a predictive mathematical model is developed by the linear regression analysis to estimate the absorptivity of EIP absorber. The laser power and scanning speed is considered variable in the model to predict absorptivity and interface temperature. The predictive equation for the absorptivity and interface temperature is shown in Eqs. (9) and (10), respectively.

$$\alpha_S = -6.86 + 0.2498 * P - 0.00937 * V \ \left(R^2 = 92.34\%\right) \tag{9}$$

$$T_{in} = -215 + 11.09 * P - 0.945 * V \ \left(R^2 = 94.67\%\right) \tag{10}$$

R^2 is the coefficient of determination that estimates the capability of the mathematical model. The value of R^2 lies between zero and one, and for a good fit, R^2 should be close to one. In the present study, the value of R^2 is found to be 0.9234 for absorptivity and 0.9467 for interface temperature. The residual plot is used to determine the significance of the coefficients in the mathematical model. The residual plot is a straight line which indicates that the residual error is normally distributed in the developed model, and the coefficients in the predictive model are significant (Fig. 20). Figure 21 shows the contour plots for the predictive response of absorptivity and interface temperature. It is seen from the figure that higher absorptivity and higher interface temperature are observed at high laser power and low scanning speed.

Nine confirmation tests are conducted at random parameter combinations to validate the predictive model by regression analysis for absorptivity. The results are compared with the estimated absorptivity at these random combinations of laser power and scanning speed by using the hybrid integrated model, as shown in Table 3. The predictive model results are observed to be in good agreement with the hybrid integrated model, and the maximum error for absorptivity is found less than 9%.

Table 3 Results of experimental confirmation test to verify regression model for absorptivity

P (W)	V (mm/min)	W_S (mm)	T_E (°C)	T_S (°C)	Error (%) in T_E and T_S	Predicted α_S (%)	Estimated α_S (%)	Error (%) in α_S
92	408	4.5	75.5	77	1.99	12.04	12	0.33
111	304	5.1	103	110	6.80	18	16.4	8.89
125	510	5	82	88	7.32	19.59	18.5	5.56
114	323	5.2	104	111	6.22	18.6	17	8.60
145	568	5.4	94	101	7.45	24	23	4.17
117	584	4.8	72.5	75	3.45	16.9	16	5.33
120	430	5.15	89	91	2.25	19	17.5	7.89
92	441	3.9	60	64	6.67	12	11	8.33
103	233	4.9	118	121	2.54	16.7	15.2	8.98

5 Conclusions

This study deals with the development of a new integrated hybrid methodology for the estimation of interface temperature and absorptivity based on inverse analysis technique in laser transmission welding. This methodology is more robust as the FEM-based numerical model is validated with experimental results by comparing weld width with tuned absorptivity and further by comparing the surface temperature with infrared thermography. The variation in heat flux with stand-off distance is also incorporated in the model to achieve more accurate computational results. The developed numerical model is validated with the experimental results, which shows good accuracy with $R^2 = 98.74\%$, and the average error is obtained less than 6%. The proposed hybrid technique predicts that the absorptivity is independent of scanning speed at low laser power. But, at high laser power, the absorptivity changes significantly with scanning speed. This approach may be suitable for estimating the absorptivity of the absorbers used in laser transmission welding and other laser-based manufacturing processes such as laser cladding, laser-based additive manufacturing, and laser welding. The accurate estimation of absorptivity also serves the purpose of estimating interface temperature at the joining interface and indicates that the interface temperature increases with line energy.

Author contribution Dhruva Kumar Goyal has proposed the methodology and performed the numerical simulations and experiments, including data analysis, and drafted the original manuscript. Ramsingh Yadav coordinated and helped in the development of experimental setup, conducting the experiments, and editing the original manuscript. Ravi Kant has supervised the overall project from conceptualization to methodology. He has reviewed and edited the primary manuscript. He also led the project and overall collaborative effort of all entities.

Availability of data and material The authors confirm that the data and material supporting the findings of this study are available within the article. Raw data are available from the corresponding author upon reasonable request.

Code availability DFLUX subroutine is written in Fortran to incorporate the moving heat flux. The subroutine code can be provided by the corresponding author upon reasonable request.

Declarations

Conflict of interest The authors declare no competing interests.

References

1. Liu M, Ouyang D, Zhao J, Li C, Sun H, Ruan S (2018) Clear plastic transmission laser welding using a metal absorber. Opt Laser Technol 105:242–248. https://doi.org/10.1108/13552540010337029

2. Liu MQ, Ouyang DQ, Li CB, Sun HB, Ruan SC (2018) Effects of metal absorber thermal conductivity on clear plastic laser transmission welding. Chin Phys Lett 35(10):104205. https://doi.org/10.1088/0256-307X/35/10/104205

3. Wu J, Lu S, Wang HJ, Wang Y, Xia FB, Jin-Wang (2021) A review on laser transmission welding of thermoplastics. Int J Adv Manuf Technol 116(7–8):2093–2109. https://doi.org/10.1007/s00170-021-07519-z

4. Pereira AB, Fernandes FAO, de Morais AB, Quintão J (2019) Mechanical Strength of Thermoplastic Polyamide Welded by Nd: YAG Laser. Polymers 11(9):1381. https://doi.org/10.3390/polym11091381

5. Acherjee B (2021) Laser transmission welding of polymers – a review on welding parameters, quality attributes, process monitoring, and applications. J Manuf Process 64:421–443. https://doi.org/10.1016/j.jmapro.2021.01.022

6. Mehrpouya M, Gisario A, Rahimzadeh A, Barletta M (2019) An artificial neural network model for laser transmission welding of biodegradable polyethylene terephthalate/polyethylene vinyl acetate (PET/PEVA) blends. Int J Adv Manuf Technol 102(5–8):1497–1507. https://doi.org/10.1007/s00170-018-03259-9

7. Villar M, Garnier C, Chabert F, Nassiet V, Samélor D, Diez JC, Sotelo A, Madre MA (2018) In-situ infrared thermography measurements to master transmission laser welding process parameters of PEKK. Opt Lasers Eng 106(February):94–104. https://doi.org/10.1016/j.optlaseng.2018.02.016

8. Becker F, Potente H (2002) A step towards understanding the heating phase of laser transmission welding in polymers. Polym Eng Sci 42(2):365–374. https://doi.org/10.1002/pen.10954

9. Horn W (2009) A progressive laser joining method: online process control with pyrometer and galvo scanner. Laser Tech J 6(1):42–43. https://doi.org/10.1002/latj.200990008

10. Ilie M, Kneip JC, Matteï S, Nichici A, Roze C, Girasole T (2007) Through-transmission laser welding of polymers - temperature field modeling and infrared investigation. Infrared Phys Technol 51(1):73–79. https://doi.org/10.1016/j.infrared.2007.02.003

11. Speka M, Matteı S, Pilloz M, Ilie M (2008) The infrared thermography control of the laser welding of amorphous polymers. Ndt E Int 41:178–183. https://doi.org/10.1016/j.ndteint.2007.10.005

12. Van De Ven JD, Erdman AG (2007) Laser transmission welding of thermoplastics – part I : temperature and pressure modeling. J Manuf Sci Eng 129:849–858. https://doi.org/10.1115/1.2752527

13. Mahmood T, Mian A, Amin MR, Auner G, Witte R, Herfurth H, Newaz G (2007) Finite element modeling of transmission laser microjoining process. J Mater Process Technol 186:37–44. https://doi.org/10.1016/j.jmatprotec.2006.11.225

14. Mayboudi LS, Birk AM, Zak G, Bates PJ (2009) A three-dimensional thermal finite element model of laser transmission welding for lap-joint. Int J Model Simul 29(2):149–155. https://doi.org/10.1080/02286203.2009.11442520

15. Acherjee B, Kuar AS, Mitra S, Misra D (2012) Modeling of laser transmission contour welding process using FEA and DoE. Opt Laser Technol 44:1281–1289. https://doi.org/10.1016/j.optlastec.2011.12.049

16. Sooriyapiragasam SK, Hopmann C (2016) Modeling of the heating process during the laser transmission welding of thermoplastics and calculation of the resulting stress distribution.

Welding in the World 60(4):777–791. https://doi.org/10.1007/s40194-016-0330-z

17. Wang C, Liu H, Chen Z, Zhao D, Wang C (2021) A new finite element model accounting for thermal contact conductance in laser transmission welding of thermoplastics. Infrared Phys Technol 112:103598. https://doi.org/10.1016/j.infrared.2020.103598

18. Acherjee B (2021) Laser transmission welding of dissimilar plastics: 3-D FE modeling and experimental validation. Weld World. https://doi.org/10.1007/s40194-021-01079-2

19. Lambiase F, Genna S (2020) Homogenization of temperature distribution at metal-polymer interface during laser direct joining. Opt Laser Technol 128:106226. https://doi.org/10.1016/j.optlastec.2020.106226

20. Wei LC, Ehrlich LE, Powell-Palm MJ, Montgomery C, Beuth J, Malen JA (2018) Thermal conductivity of metal powders for powder bed additive manufacturing. Addit Manuf 21:201–208. https://doi.org/10.1016/j.addma.2018.02.002

21. Kant R, Joshi SN (2016) Numerical and experimental studies on the laser bending of magnesium M1A alloy. Lasers Eng 35(1–4):39–62

22. Wahba M, Kawahito Y, Katayama S (2011) Laser direct joining of AZ91D thixomolded Mg alloy and amorphous polyethylene terephthalate. J Mater Process Technol 211(6):1166–1174. https://doi.org/10.1016/j.jmatprotec.2011.01.021

23. Tolochko NK, Khlopkov YV, Mozzharov SE, Ignatiev MB, Laoui T, Titov VI (2000) Absorptance of powder materials suitable for laser sintering. Rapid Prototyp J 6(3):155–160. https://doi.org/10.1108/13552540010337029

24. Goyal D.K, Yadav R, Kant R (2022) Study of Temperature Field Considering Gradient Volumetric Heat Absorption in Transparent Sheet During Laser Transmission Welding (LTW). Lasers Eng 53(3–4):215–229